

Interaction Studies between Carbonic Anhydrase and a Sulfonamide Inhibitor by Experimental and Theoretical Approaches

Daniela Pagnozzi, Nicolino Pala, Grazia Biosa, Roberto Dallochio, Alessandro Dessì, Pankaj Kumar Singh, Dominga Rogolino, Anna Di Fiore, Giuseppina De Simone, Claudiu T. Supuran,* and Mario Sechi*



Cite This: *ACS Med. Chem. Lett.* 2022, 13, 271–277



Read Online

ACCESS |



Metrics & More



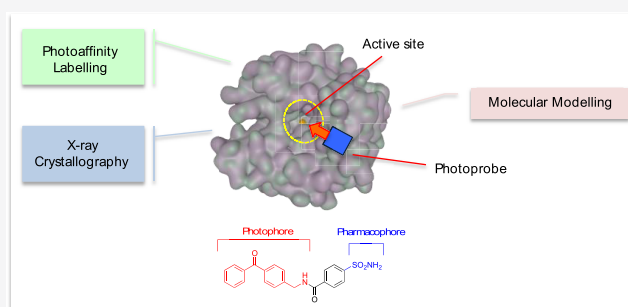
Article Recommendations



Supporting Information

ABSTRACT: The most used approaches in structure-based drug design possess peculiar characteristics with advantages and limitations, and thus the management of complementary data from various techniques is of particular interest to synergistically achieve the development of effective enzyme inhibitors. In this Letter, we describe the application of experimental and computational techniques to study the interactions between human carbonic anhydrases and sulfonamide inhibitors. In particular, a series of affinity-labeled carbonic anhydrase inhibitors containing sulfonamido photoprobes was designed and synthesized, and one of these compounds, a benzophenone derivative, was chosen as a model photoprobe/inhibitor. A photoaffinity labeling method followed by mass spectrometry analysis was then applied to elucidate the inhibitor binding site, and a comparison with X-ray crystallography and molecular dynamics simulation data was carried out, highlighting that to have a comprehensive view of the protein/inhibitor complex stabilization all three kinds of experiments are necessary.

KEYWORDS: Carbonic anhydrase, sulfonamides, molecular recognition, photoaffinity labeling, X-ray crystallography, molecular modeling



Structure-based drug design (SBDD) is one of the most innovative and powerful strategies in drug development.¹ It requires the availability of the 3D structure of the target under study in complex with an existing inhibitor² and an understanding of the principles of molecular interaction in protein–ligand complexes. Thus X-ray crystal structures of ligands in complex with the target protein have been, for a long period, an important tool for medicinal chemists in the discovery, design, and optimization of prototypes of drug candidates.^{3–5} However, as the role of dynamics gained importance in the function of proteins, the limitations of X-ray crystallography to not be able to capture this behavior came to the forefront.⁶ This is a crucial issue in the analysis of processes that involve conformational changes or in the evaluation of molecular binding interactions and energies. Despite this, nuclear magnetic resonance (NMR)-based techniques are valuable methods for studying ligands and protein structures and protein–ligand interactions and dynamics in solution.⁷ Molecular dynamics (MD) simulations also aim to predict the dynamic evolution of a molecular system over the time.⁸

In this context, photoaffinity labeling (PAL), that is, the “capture” of proteins by small molecules via photoactivation-mediated irreversible cross-linking and subsequent analysis by tandem mass spectrometry (MS), recently emerged as a highly useful technique for identifying sites of molecular interactions

and a powerful method in the structural proteomic approach for protein function evaluation.^{9–11} This technique relies on the incorporation of a chemical functionality that is inert until specific light activation into the ligand (inhibitor) of interest.⁹ Within a macro-level stage, PAL can be used to identify binding sites in target proteins, and such information can address the biomolecular screening of drug prototype candidates. Second, a micro-level exploration could be pursued by digestion of the labeled protein into short peptides to localize the specific binding region and, eventually, the amino acids involved in the binding interactions.⁹ Where crystallographic structural analysis is difficult to manage, PAL provides a helpful method to achieve the identification of the molecular binding site.

Recently, we reported the incorporation of photoreactive groups into diketoacid (DKA)-based HIV-integrase (IN) inhibitors for the identification of the DKA binding site on

Received: November 14, 2021

Accepted: January 13, 2022

Published: January 31, 2022



the IN protein.¹² Continuing this kind of study, in this Letter, we aimed at evaluating the potential of this approach to obtain information on the molecular recognition process between human carbonic anhydrases (hCAs) and sulfonamide inhibitors.

hCAs are a family of zinc enzymes that catalyze the reversible hydration of carbon dioxide to bicarbonate and proton.¹³ So far, 15 different hCAs have been identified that show different catalytic activities, subcellular localizations, and tissue distributions. Some hCA isoforms are recently emerging as potential biological targets and are involved in the regulation of different physiopathological events.¹³ CA inhibitors (CAIs) such as sulfonamides and their bioisosteres, sulfamates and sulfamides, are the ideal chemotypes for efficiently binding within the enzyme active site, and some of them are well-validated drugs or are currently in developmental stages.¹⁴

Although many X-ray crystallographic structures of hCA/inhibitor complexes are available so far, showing the key interactions responsible for the protein–inhibitor complex stabilization within the active site, further insights could be useful for clarifying the binding mode of CAIs through the determination of dynamic parameters, for example, through PAL and molecular modeling tools (Figure 1), and for identifying other sites of action, in particular, for the most interesting isoforms.

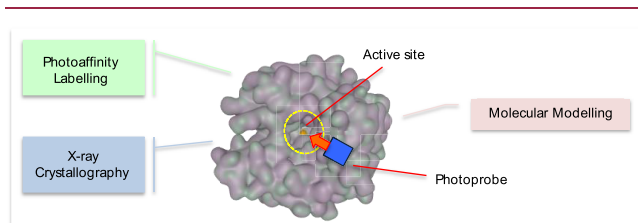


Figure 1. Study design: investigation of hCA/inhibitor interactions by complementary approaches.

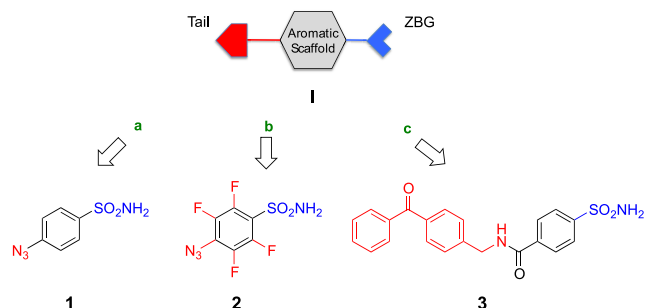
To date, few studies have reported the incorporation of photoreactive groups into sulfonamide-based CAIs; in particular, these agents were used for the identification of an intracellular CA in a green alga,¹⁵ for a photomediated CA II capture and visualization by fluorescence,¹⁶ and for facile conjugation to protein-binding (CA IX and TrkC) ligands.¹⁷ However, no comprehensive study has been reported so far on the use of the PAL approach and MS analysis¹⁸ in combination with the previously mentioned experimental methods to characterize a CAI binding site.

Herein we report the design and synthesis of CAIs containing sulfonamido photoprobes and the characterization of their binding site by using complementary techniques such as the PAL method followed by MS analysis, X-ray crystallography, and MD simulations.

The starting idea that inspired the photoprobe design was to create compounds with a good inhibition capacity toward hCAs, that is, compounds containing the minimal structural requirements foreseen for the activity of classical inhibitors. We focused our attention on sulfonamide inhibitors; these molecules are generally characterized by the presence of three main structural elements: the sulfonamide moiety, which acts as zinc binding group (ZBG), an aromatic scaffold that interacts with the lower-middle region of the active site, and one or more “tails” that interact with the outer region of the catalytic cavity and are responsible of the isoform selectivity, as

the outer region of the active site is the most variable one among the various hCAs.^{19,20} Thus for our purpose, the para-substituted benzene-sulfonamide structure derived from a classical CAI was chosen as the general scaffold for the photoprobes (Chart 1). A phenylazido function (a), its

Chart 1. Designed Photoprobes 1–3 from the Structure of a Classical CAI^a



^aPhotophores and pharmacophores are highlighted in red and blue, respectively.

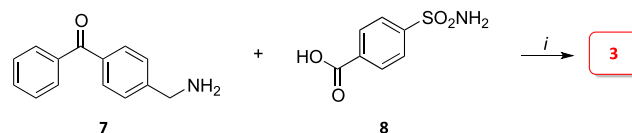
polyfluorinated analogue (b), and a benzophenone-based group (c) were selected as well-known photophores on the basis of their photoreactive functionalities and were incorporated into I to give photoprobes 1–3 (Chart 1).

Photoprobe 1 was synthesized under mild conditions by direct azidation of the aminosulphanilamide (4) with sodium azide in *t*-butanol and *t*-butyl nitrite (Scheme S1).

The synthesis of photoprobe 2 (the polyfluorinated analogue of 1) was carried out by substitution in position 4 of pentafluorobenzenesulfonamide (6) with sodium azide in a mixture of water and acetone under reflux. The intermediate 6 was obtained starting from pentafluorosulfonyl chloride (5), which is commercially available, by treatment with concentrated NH₄OH (Scheme S2).

Finally, photoprobe 3 was obtained in good yield by the amidation of the intermediate 7¹² and *p*-sulfamoylcarboxylic acid (8) in the presence of 1-ethyl-3-(3-dimethylaminopropyl)carbodiimide (EDC) and *N*-hydroxybenzotriazole (Scheme 1).

Scheme 1. Synthetic Route for the Preparation of 3^a



^aReagents and conditions: EDC, HOBT, DMA/CH₂Cl₂, r.t. for 6 h.

The optimal approach for the synthesis of the intermediate *p*-methylamino benzophenonic 7 involved the bromination of *p*-methylbenzophenone (9) with *N*-bromosuccinimide, catalyzed by dibenzoylperoxide, in CCl₄ at reflux. The thus-obtained intermediate 10 was converted into amino derivative 7 by treatment with sodium azide in dimethylformamide (DMF) at room temperature (r.t.) to give 11 followed by a reduction according to Staudinger using triphenylphosphine in a methanol/water mixture (Scheme S3).

Photoprobes 1–3 were assayed *in vitro* for their inhibitory action against the 12 catalytically active hCA isoforms by

means of a stopped-flow CO₂ hydrase assay. The obtained results are summarized in Table 1 and compared with K_i values of the clinically used drug acetazolamide (AZA).

Table 1. Inhibition Data of Photoprobes 1–3 against hCA I–XIV by a Stopped-Flow CO₂ Hydrase Assay^a

isoform/ K_i (nM)	1	2	3	AZA
hCA I	1015	929	1166	250
hCA II	92	88	1050	12
hCA III	34000	26500	64800	20000
hCA IV ^b	513	468	724	74
hCA VA	904	817	967	63
hCA VB	865	792	915	54
hCA VI	784	688	917	11
hCA VII	64	56	806	2.5
hCA IX ^b	66	59	977	25
hCA XII ^b	87	79	1020	5.7
hCA XIII	396	180	640	18
hCA XIV ^b	858	684	995	41

^aMean from three different assays by a stopped-flow technique (errors are in the range of 5–10% of the reported values). ^bCatalytic domains were used for inhibition measurements. AZA, acetazolamide (standard drug).

In general, all compounds inhibited the catalytic activity of all isoforms, except for hCA III (although in line with AZA), in the nanomolar/low micromolar range ($K_i = 56$ to 1166 nM). Compounds 1 and 2 showed similar inhibitory profiles, whereas 3 displayed a different K_i value against the tested isoforms, thus confirming that the nature of the para substituent on the benzene-sulfonamide structure significantly influenced the inhibition potency.

Because of its well-known investigation and experimental manageability, isoform II was chosen as the protein model for PAL. All three photoprobes displayed good inhibition properties for this isoform with K_i values of 92, 88, and 1050 nM for compounds 1, 2, and 3, respectively, thus making all of them suitable to be used for microlevel PAL analysis.

The average mass of free hCA II was measured by MS analysis, and an experimental value of $29\,156.66 \pm 0.24$ Da was obtained, confirming the expected value according to the sequence deposited on UniProtKB (entry P00918, 259 residues, with N-terminal serine modified as *N*-acetylserine) (theoretical average mass = 29 156.84 Da).

The photoprobe MS analysis evidenced a relative instability of 1 and 2, and thus these compounds were found to be unsuitable for the next stages of PAL analysis, and only photoprobe 3 was considered. Indeed, although the most active compound resulted in *p*-azidobenzensulfonamide 2 (K_i hCA II = 88 nM), and even if an optimal activity of the photoprobe was required for a successful PAL experiment, several examples are available in the literature describing photoprobes with markedly lower activities than “ancestor compounds”, even when they possess inhibition potency in the micromolar range of concentration. In addition, compounds containing a benzophenone chemotype demonstrate a greater chemical stability under normal conditions compared with other photophores and can be manipulated even in the presence of ambient light without running the risk of triggering protein degradation processes.⁹ In addition, by exploiting the highly electrophilic character of the carbonyl in the excited state, these compounds are also able to react with generally

inert bonds, and photoactivation occurs at a wavelength that does not affect the structural integrity of the target.

The MS experiments of photoprobe 3 revealed the existence of the pseudomolecular MH^+ ions corresponding to different oligomeric states. More specifically, the spectrum showed the monomeric species, but also dimeric, trimeric, and tetrameric species were present (Table S1, Figure S1).

A cross-linking reaction was performed by irradiating photoprobe 3 incubated with hCA II at 366 nm using a UV apparatus. The PAL products were first desalted and analyzed by MS of the single reversed-phase high-performance liquid chromatography (RP-HPLC) fraction. The spectrum revealed the presence of the unreacted photoprobe, its dimeric, trimeric, and tetrameric forms, and the multicharged ion distribution of the unreacted CA II and of the CA II–photoprobe 3 complex (Figure 2).

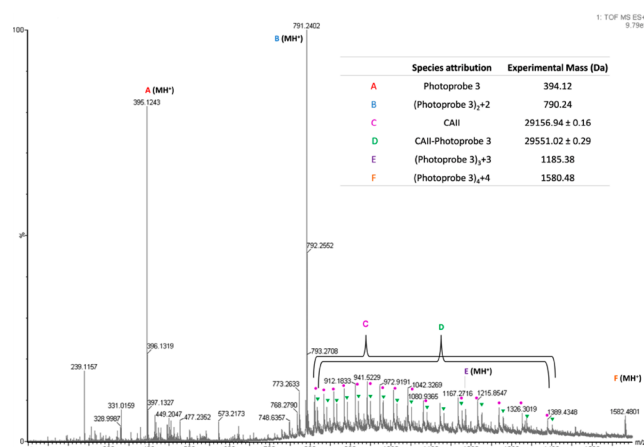


Figure 2. Time-of-flight mass spectrometry (TOF-MS) spectrum of the photoaffinity labeling products and unreacted species. A, B, E, and F correspond to the MH^+ of monomeric, dimeric, trimeric, and tetrameric structures of unreacted photoprobe 3, respectively. C and D are the multicharged distributions of unreacted CA II protein and of the CA II–photoprobe 3 complex, respectively.

Interestingly, the m/z of the unreacted photoprobe was perfectly consistent with the theoretical value, whereas the ions corresponding to dimeric, trimeric, and tetrameric structures differed from the theoretical MH^+ ions of 2, 3, and 4 Da, respectively (Figure 2).

These results suggest the addition of two, three, and four hydrogen atoms to the dimeric, trimeric, and tetrameric molecules, respectively. The multicharged ion distribution of the protein–inhibitor complex gave an average mass corresponding to the sum of CA II and photoprobe 3 ($m/z = 29\,551.02$, Figure 2).

The complex was digested and analyzed by LC-MS/MS to assign the residue directly involved in the photoaffinity reaction. The analysis of the tandem MS spectrum of the doubly charged precursor ion with $m/z = 1032.038$ ($MH^+ = 2063.068$) allowed the identification of the protein sequence involved in the cross-link.²¹ In more detail, the fragmentation spectrum led to the attribution of peptides 134–149 (according to the sequence of PDB 2ILL,²² shown in Figure S2) ($MH^+_{\text{theoretical}} = 1668.961$) as the ones modified by a mass of 394.1 Da, corresponding to compound 3. According to the *a* and *b* series, alanine 134 was identified as the amino acid linked to photoprobe 3 (Figure 3).

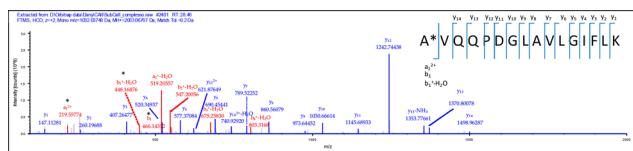


Figure 3. Electrospray ionization–higher-energy C-trap dissociation (HCD) spectrum of peptide amino acids 134–149 in the protein sequence. The MH_2^{2+} signal at 1032.037 m/z was selected as a precursor ion. Symbol * on the amino acid sequence shows the modified residue.

The main features of the binding between photoprobe **3** and the hCA II active site were also analyzed by means of a detailed crystallographic study. Crystals of the hCA II/3 adduct were obtained by cocrystallization experiments following a protocol well described in the literature.²⁵ The crystal structure of this complex was determined at 1.70 Å (PDB 7NTB) and refined to R-work and R-free values of 17.3 and 21.7%, respectively. (See Table S2 for the data collection and refinement statistics.) The refined structure presented a good geometry with a root-mean square deviation (rmsd) from ideal bond lengths and angles of 0.009 Å and 1.5°, respectively.

The analysis of the electron density maps around the catalytic site showed features compatible with the presence of one inhibitor molecule bound within the hCA II active-site cavity (Figure 4).

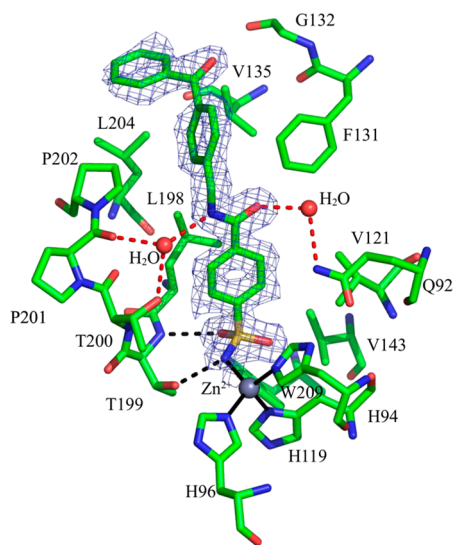


Figure 4. Sigma-A-weighted $|2F_o - F_c|$ simulated annealing omit map (contoured at 1.0 σ) of inhibitor **3** bound to the hCA II active site. The catalytic zinc ion is represented as a gray sphere. The zinc ion coordination (black continuous lines), hydrogen bonds (black dashed lines), and residues involved in van der Waals interactions are also depicted.

Inhibitor binding did not alter the hCA II three-dimensional structure,^{24,25} as indicated by the low rmsd value calculated by the superposition of all of the $C\alpha$ atoms of the hCA II/3 adduct with those of the unbound enzyme (rmsd value of 0.25 Å).

Active-site analysis showed that the sulfonamide moiety presents a binding mode to hCA II similar to that observed for other CAIs containing the same group.²⁰ In particular, the deprotonated nitrogen atom displaces the hydroxyl ion/water molecule found in the native enzyme and coordinates the zinc

metal ion with a tetrahedral geometry, while further hydrogen-bond interactions between the sulfonamide moiety and the Thr199 residue contribute to stabilizing the binding (Figure 4). In addition, the acetamide moiety forms water-mediated hydrogen bonds with Gln92, Thr200, and Pro201. Several strong van der Waals interactions (<4.0 Å) stabilize the hCA II/3 complex. In particular, the benzenesulfonamide core interacts with Gln92, His94, His96, His119, Val121, Val143, Leu198, Thr200, and Trp209, whereas the acetamido group interacts with Phe131. Finally, the benzophenone functionality is located at the entrance of the hCA II active site cavity and is stabilized by the formation of van der Waals contacts with Gly132, Val135, Pro202, and Leu204 amino acids. Surprisingly the distance between the Ala134 carbon atom and the carbonyl carbon of the benzophenone moiety was rather long (8.5 Å), thus making it difficult to foresee the formation of the chemical bond between these groups after photoactivation, as unveiled from the PAL experiment.

To complete our analysis, we analyzed the binding mode between photoprobe **3** and hCA II by MD simulations. To this aim, compound **3** was constructed with standard bond lengths and angles from the fragment database with MacroModel^{26,27} and docked in the CA II active site (PDB ID: 2ILI,²² which overlapped with the sequence of our solved hCA II/3 complex, Figure S3). The conformation maintaining a better interaction within the catalytic site was selected and subjected to MD simulations for a time of 100 ns, and molecular mechanics energies combined with the generalized Born or Poisson–Boltzmann and surface-area continuum solvation (MM/PBSA and MM/GBSA) methods were used to determine the binding energies. Analysis of the trajectories revealed that the inhibitor sulfonamide group maintains the key interactions with the enzyme catalytic site during all simulation times (Figure 5A).

Indeed, the distance between the nitrogen atom of the sulfonamide functionality and the Zn^{2+} ion throughout the simulation period retains an almost constant value of 2 Å, in agreement with N– Zn^{2+} distances observed in the crystallographic structures of protein/inhibitor complexes reported so far.²⁰ Additionally, the rmsd values of the protein backbone atoms revealed the complex to be fairly stable immediately after 4 ns until the completion of the simulations (Figure 5B).

To explain discrepancies observed between PAL and X-ray data, particular attention was dedicated to the study of the interaction features between the photophore substructure and Ala134/Val135 residues during MD simulations.²⁸ Interestingly, MD simulations revealed that the benzophenone moiety of **3** was in close contact with both residues. In detail, during the initial time frames (~ 10 ns), the benzophenone moiety moved toward Val135 and Ala134; however, at later time frames, it moved slightly away (see Figure 6, plot 40–70 ns). The plot of distance versus time between the carbonyl carbon of the benzophenone and Val135/Ala134 residues disclosed that after the initial adjustment of the complex, the photoprobe atom remained in close contact with Val135 with an average distance of 5 Å and more distant from Ala134 with an average distance of 9 Å (Figures 5C and 6), in agreement with what was observed by X-ray crystallography but not aligned with the results of the PAL experiment.

However, it should be considered that MD simulations, being a molecular mechanics approach, do not consider the possibility of bond breakage and bond formation and thus cannot mimic the effect of photoactivation on the interaction of the photophore and surrounding residues.

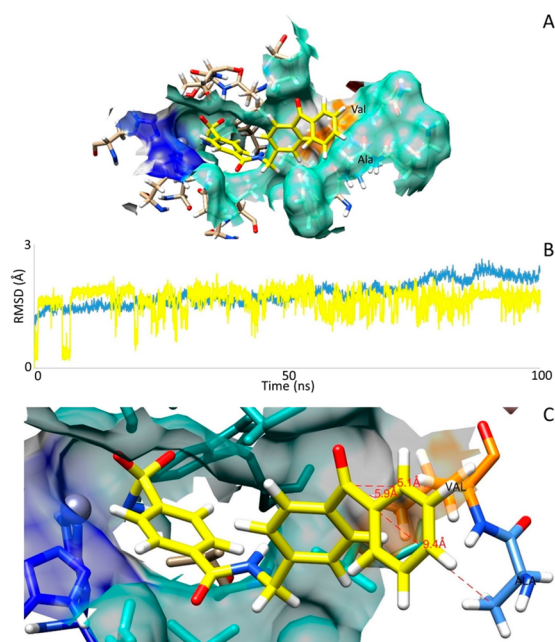


Figure 5. (A) Binding mode of photoprobe 3 within the CA II catalytic site after MD simulations for 100 ns. The amino acid residues interacting with the probe are shown. Zn^{2+} ions (gray) and histidine residues are highlighted. (B) rmsd computed on protein backbone atoms (blue) and photoprobe 3 heavy atoms (yellow) during simulation. (C) Detail of the interaction between methyl groups on the side chain of Val135 (orange) or Ala134 (blue) and the carbonyl carbon of the photoprobe 3 benzophenone.

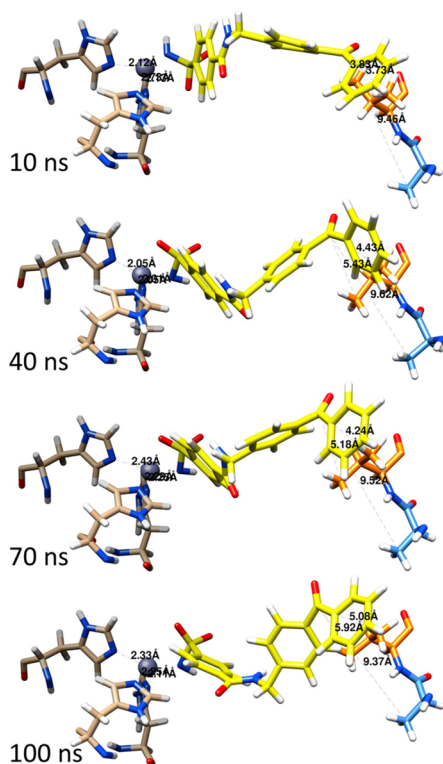


Figure 6. Evolution of time frames from 0 to 100 ns for the MD of photoprobe 3 in the hCA II active site. Distance versus time between residues Val135 (pale orange) or Ala134 (blue) and the photoprobe carbonyl carbon is shown. Zinc cofactor (gray) and histidine residues are highlighted.

A detailed understanding of the essential interactions making use of complementary methods and protocols is thus emerging for careful protein/ligand complex stabilization studies. In this work, we used a combined approach consisting of PAL experiments followed by MS analysis, X-ray crystallography, and MD simulations to obtain a complete overview of the molecular interactions between a classical sulfonamide inhibitor and hCA II.

First, by means of X-ray crystallography, a classical technique to study a static situation, we observed the interaction of the benzophenone inhibitor moiety with hCA II residues Gly132, Val135, Pro202, and Leu204. MD simulations, a computational technique very useful in the examination of protein dynamic behavior, highlighted a certain degree of flexibility of the inhibitor within the active site.

Finally, PAL experiments, which involved a photoactivation-mediated cross-linking followed by MS analysis, highlighted a more dynamic behavior of the protein/inhibitor complex with respect to what was observed with X-ray crystallography and MD simulations.

Indeed, PAL experiments showed the formation of a chemical bond between the inhibitor benzophenone moiety and the hCA II Ala134 residue, which, from the previous techniques, were shown to be rather distant, thus indicating a higher flexibility of the inhibitor within the active site with respect to what was foreseen by classical structural investigations.

Altogether, these data strongly suggest that to have a comprehensive view of the protein/inhibitor molecular recognition process, complementary techniques have to be taken into account to better describe the complex and dynamic scenario of the interaction between the target protein and its inhibitor.

■ ASSOCIATED CONTENT

Supporting Information

The Supporting Information is available free of charge at <https://pubs.acs.org/doi/10.1021/acsmmedchemlett.1c00644>.

Synthesis of photoprobes 1, 2, and intermediate 7 (S3). MS spectrum of photoprobe 3 (S4). Spectrum signals from MS analysis of photoprobe 3 (S5). Sequence of hCA II (S5). Data collection and refinement statistics for hCA II/3 complex (S6). Experimental methods (S7). Synthesis and characterization details of photoprobes 1–3 (S8–S11). CA inhibition studies (S12). Mass spectrometry analysis of hCA II and the photoprobe 3 (S13). Photoaffinity labeling of CA II (S14). Purification of the hCA II-3 complex by RP-HPLC (S14). Tryptic digestion of the hCA II/3 complex and LC-MS/MS analysis (S14 and S15). Crystallization, X-ray data collection, and refinement (S16). In silico analysis: preparation of photoprobe 3 (S17). Molecular docking (S17). Superposition of PDB 2ILI and 7NTB (S18). Molecular dynamics (S19 and S20) (PDF). Compounds in SMILES format (PDF).

■ AUTHOR INFORMATION

Corresponding Authors

Mario Sechi – Department of Medical Surgical and Experimental Sciences, University of Sassari, 07100 Sassari, Italy; Present Address: Department Chemistry and Pharmacy, University of Sassari, Via Vienna 2, 07100

Sassari, Italy; orcid.org/0000-0003-2983-6090;
Phone: +39 079-228-753; Email: mario.sechi@uniss.it
Claudiu T. Supuran – Polo Scientifico, Neurofarba
Department and Laboratorio di Chimica Bioinorganica,
Università degli Studi di Firenze, 50019 Florence, Italy;
orcid.org/0000-0003-4262-0323; Phone: +39-055-
4573729; Email: claudiu.supuran@unifi.it

Authors

Daniela Pagnozzi – Porto Conte Ricerche, Science and
Technology Park of Sardinia, 07041 Alghero, Sassari, Italy
Nicolino Pala – Department of Chemistry and Pharmacy,
University of Sassari, 07100 Sassari, Italy
Grazia Biosa – Porto Conte Ricerche, Science and Technology
Park of Sardinia, 07041 Alghero, Sassari, Italy
Roberto Dallochio – Istituto di Chimica Biomolecolare -
CNR, 07100 Sassari, Italy
Alessandro Dessì – Istituto di Chimica Biomolecolare - CNR,
07100 Sassari, Italy; orcid.org/0000-0001-8258-7332
Pankaj Kumar Singh – Department of Chemistry and
Pharmacy, University of Sassari, 07100 Sassari, Italy;
orcid.org/0000-0002-4774-6358
Dominga Rogolino – Department of Chemistry, Life Sciences
and Environmental Sustainability, University of Parma,
43124 Parma, Italy; orcid.org/0000-0003-2295-5783
Anna Di Fiore – Istituto di Biostrutture e Bioimmagini-CNR,
80134 Naples, Italy
Giuseppina De Simone – Istituto di Biostrutture e
Bioimmagini-CNR, 80134 Naples, Italy; orcid.org/0000-0001-9783-5431

Complete contact information is available at:
<https://pubs.acs.org/10.1021/acsmmedchemlett.1c00644>

Notes

The authors declare no competing financial interest.

ACKNOWLEDGMENTS

D.P. was supported by Sardegna Ricerche, Science and Technology Park of Sardinia, under grant program art.9 LR 20/2015 to Porto Conte Ricerche. This research was also financed by the Italian Ministry of Research and University (MIUR), grant PRIN: prot. 2017XYBP2R (to C.T.S.). We thank Mr. Maurizio Amendola for his skillful technical assistance with X-ray measurements. M.S. was partially supported by FAR2020.

ABBREVIATIONS

CA, carbonic anhydrase; hCA, human carbonic anhydrase; CAI, carbonic anhydrase inhibitor; PAL, photoaffinity labeling; MD, molecular dynamics; AZA, acetazolamide; MS, mass spectrometry

REFERENCES

- (1) Wang, X.; Song, K.; Li, L.; Chen, L. Structure-based drug design strategies and challenges. *Curr. Top. Med. Chem.* **2018**, *18* (12), 998–1006.
- (2) Batool, M.; Ahmad, B.; Choi, S. A structure-based drug discovery paradigm. *Int. J. Mol. Sci.* **2019**, *20* (11), 2783.
- (3) Neamati, N.; Barchi, J. J., Jr. New paradigms in drug design and discovery. *Curr. Top. Med. Chem.* **2002**, *2*, 211–227.
- (4) Hughes, J. P.; Rees, S.; Kalindjian, S. B.; Philpott, K. L. Principles of early drug discovery. *Br. J. Pharmacol.* **2011**, *162* (6), 1239–1249.

- (5) Cooper, D. R.; Porebski, P. J.; Chruszcz, M.; Minor, W. X-ray crystallography: assessment and validation of protein–small molecule complexes for drug discovery. *Expert Opin. Drug Discovery* **2011**, *6* (8), 771–782.
- (6) Srivastava, A.; Nagai, T.; Srivastava, A.; Miyashita, O.; Tama, F. Role of computational methods in going beyond X-ray crystallography to explore protein structure and dynamics. *Int. J. Mol. Sci.* **2018**, *19* (11), 3401.
- (7) Pellecchia, M.; Meiningner, D.; Dong, Q.; Chang, E.; Jack, R.; Sem, D. S. NMR-based structural characterization of large protein–ligand interactions. *Journal of biomolecular NMR* **2002**, *22* (2), 165–173. (b) Cala, O.; Guillièrre, F.; Krimm, I. NMR-based analysis of protein–ligand interactions. *Anal. Bioanal. Chem.* **2014**, *406* (4), 943–956.
- (8) Klepeis, J. L.; Lindorff-Larsen, K.; Dror, R. O.; Shaw, D. E. Long-timescale molecular dynamics simulations of protein structure and function. *Curr. Opin. Struct. Biol.* **2009**, *19* (2), 120–127.
- (9) Dormán, G.; Prestwich, G. D. Using photolabile ligands in drug discovery and development. *Trends Biotechnol.* **2000**, *18* (2), 64–77.
- (10) Hatanaka, Y.; Sadakane, Y. Photoaffinity labeling in drug discovery and developments: chemical gateway for entering proteomic frontier. *Curr. Top. Med. Chem.* **2002**, *2* (3), 271–288.
- (11) Smith, E.; Collins, I. Photoaffinity labeling in target-and binding-site identification. *Future Med. Chem.* **2015**, *7* (2), 159–183.
- (12) Pala, N.; Esposito, F.; Tramontano, E.; Singh, P. K.; Sanna, V.; Carcelli, M.; Haigh, L. D.; Satta, S.; Sechi, M. Development of a Raltegravir-based Photoaffinity Labeled Probe for Human Immunodeficiency Virus-1 Integrase Capture. *ACS Med. Chem. Letters* **2020**, *11*, 1986–1992.
- (13) Supuran, C. T.; Scozzafava, A.; Conway, J. *Carbonic Anhydrase: Its Inhibitors and Activators*; CRC Press: 2004; Vol. 1. (b) Ferry, J. G. The γ class of carbonic anhydrases. *Biochim. Biophys. Acta - Proteins Proteom.* **2010**, *1804* (2), 374–381.
- (14) Supuran, C. T. Carbonic Anhydrases: Novel Therapeutic Applications for Inhibitors and Activators. *Nat. Rev. Drug Discovery* **2008**, *7*, 168–181.
- (15) Sültemeyer, D. Carbonic anhydrase in eukaryotic algae: characterization, regulation, and possible function during photosynthesis. *Can. J. Bot.* **1998**, *76* (6), 962–972.
- (16) Sarathi Addy, P.; Saha, B.; Pradeep Singh, N. D.; Das, A. K.; Bush, J. T.; Lejeune, C.; Schofield, C. J.; Basak, A. 1, 3, 5-Trisubstituted benzenes as fluorescent photoaffinity probes for human carbonic anhydrase II capture. *Chem. Commun.* **2013**, *49* (19), 1930–1932.
- (17) Kue, C. S.; Kamkaew, A.; Voon, S. H.; Kiew, L. V.; Chung, L. Y.; Burgess, K.; Lee, H. B. Tropomyosin receptor kinase C targeted delivery of a peptidomimetic ligand-photosensitizer conjugate induces antitumor immune responses following photodynamic therapy. *Sci. Rep.* **2016**, *6*, 37209.
- (18) Nguyen, G. T. H.; Tran, T. N.; Podgorski, M. N.; Bell, S. G.; Supuran, C. T.; Donald, W. A. Nanoscale Ion Emitters in Native Mass Spectrometry for Measuring Ligand-Protein Binding Affinities. *ACS Cent. Sci.* **2019**, *5* (2), 308–318.
- (19) De Simone, G.; Bua, S.; Supuran, C. T.; Alterio, V. Benzyl alcohol inhibits carbonic anhydrases by anchoring to the zinc coordinated water molecule. *Biochem. Biophys. Res. Commun.* **2021**, *548*, 217–221.
- (20) Alterio, V.; Di Fiore, A.; D'Ambrosio, K.; Supuran, C. T.; De Simone, G. Multiple binding modes of inhibitors to carbonic anhydrases: how to design specific drugs targeting 15 different isoforms? *Chem. Rev.* **2012**, *112* (8), 4421–4468.
- (21) Tanca, A.; Biosa, G.; Pagnozzi, D.; Addis, M. F.; Uzzau, S. Comparison of detergent-based sample preparation workflows for LTQ-Orbitrap analysis of the Escherichia coli proteome. *Proteomics* **2013**, *13*, 2597–2607.
- (22) Fisher, S. Z.; Maupin, C. M.; Budayova-Spano, M.; Govindasamy, L.; Tu, C.; Agbandje-McKenna, M.; Silverman, D. N.; Voth, G. A.; McKenna, R. Atomic crystal and molecular dynamics simulation structures of human carbonic anhydrase II: insights into

the proton transfer mechanism. *Biochemistry* **2007**, *46* (11), 2930–2937.

(23) Di Fiore, A.; Scozzafava, A.; Winum, J.-Y.; Montero, J.-L.; Pedone, C.; Supuran, C. T.; De Simone, G. Carbonic anhydrase inhibitors: binding of an antiglaucoma glycosyl-sulfanilamide derivative to human isoform II and its consequences for the drug design of enzyme inhibitors incorporating sugar moieties. *Bioorg. Med. Chem. Lett.* **2007**, *17* (6), 1726–1731.

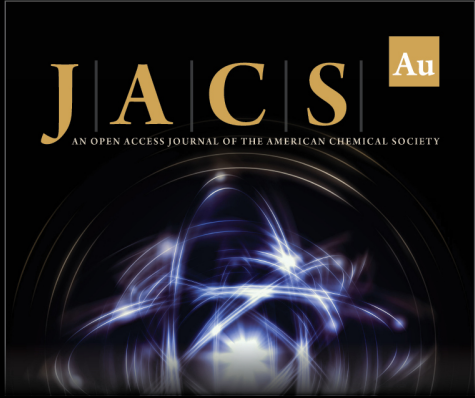
(24) Eriksson, A. E.; Jones, T. A.; Liljas, A. Refined structure of human carbonic anhydrase II at 2.0 Å resolution. *Proteins*. **1988**, *4* (4), 274–282.

(25) Otwinowski, Z.; Minor, W. Processing of X-ray diffraction data collected in oscillation mode. *Methods Enzymol.* **1997**, *276*, 307–326.


(26) Mohamadi, F.; Richards, N. G.; Guida, W. C.; Liskamp, R.; Lipton, M.; Caufield, C.; Chang, G.; Hendrickson, T.; Still, W. C. MacroModel—an integrated software system for modeling organic and bioorganic molecules using molecular mechanics. *J. Comput. Chem.* **1990**, *11* (4), 440–467.


(27) Wang, J.; Wolf, R. M.; Caldwell, J. W.; Kollman, P. A.; Case, D. A. Development and testing of a general amber force field. *J. Comput. Chem.* **2004**, *25* (9), 1157–1174.


(28) Case, D. A.; Darden, T. A.; Cheatham, T. r.; Simmerling, C. L.; Wang, J.; Duke, R. E.; Luo, R.; Walker, R. C.; Zhang, W.; Merz, K. M. *Amber 11*; University of California: 2010.



JACS Au
AN OPEN ACCESS JOURNAL OF THE AMERICAN CHEMICAL SOCIETY

 Editor-in-Chief
Prof. Christopher W. Jones
Georgia Institute of Technology, USA

Open for Submissions 

pubs.acs.org/jacsau  ACS Publications
Most Trusted. Most Cited. Most Read.